

# Structural trends from a consistent set of single-crystal data of $REFeAsO$ ( $RE = La, Ce, Pr, Nd, Sm, Gd, \text{ and } Tb$ )

F. Nitsche,<sup>1</sup> A. Jesche,<sup>2</sup> E. Hieckmann,<sup>3</sup> Th. Doert,<sup>1</sup> and M. Ruck<sup>1,2</sup>

<sup>1</sup>*Department of Chemistry and Food Chemistry, Technische Universität Dresden, D-01062 Dresden, Germany*

<sup>2</sup>*Max Planck Institute for Chemical Physics of Solids, D-01187 Dresden, Germany*

<sup>3</sup>*Institute of Applied Physics, Technische Universität Dresden, D-01062 Dresden, Germany*

(Dated: October 14, 2010)

A new crystal growth technique for single-crystals of  $REFeAsO$  ( $RE = La, Ce, Pr, Nd, Sm, Gd, \text{ and } Tb$ ) using  $NaI/KI$  as flux is presented. Crystals with a size up to  $300\mu m$  were isolated for single-crystal X-ray diffraction measurements. Lattice parameters were determined by LeBail fits of X-ray powder data against  $LaB_6$  standard. A consistent set of structural data is obtained and interpreted in a hard-sphere model. Effective radii for the rare-earth metal atoms for  $REFeAsO$  are deduced. The relation of the intra- and inter-plane distances of the arsenic atoms is identified as limiter of the phase formation, and its influence on  $T_c$  is discussed.

PACS numbers: 61.66.Fn, 74.62.Bf, 74.70.Xa, 81.10.Dn

Keywords:  $REFeAsO$ , single crystal, Fe-based superconductors, transport properties, flux, crystal growth

## I. INTRODUCTION

The discovery of superconductivity in the system  $LaFePO(F)$  by Kamihara *et al.*<sup>1</sup> and the subsequent examination of various compounds with a square iron-net substructure such as  $REFeAsO$  ( $RE$ -1111 with  $RE = \text{rare-earth metal}$ ),  $AFe_2As_2$  ( $A$ -122 with  $A = Ca, Sr, Ba \text{ and } Eu$ ),  $BFeAs$  ( $B$ -111 with  $B = Li, Na, K$ ),  $FeCh$  (11 with  $Ch = Se_{1-x}Te_x$ ) revealed a large set of structures and options of doping to study superconductivity.

In the  $REFeAsO$  compounds, which crystallize in the  $ZrCuSiAs$  structure type (Fig. 1), superconductivity can be achieved by electron<sup>2</sup> and hole<sup>3</sup> doping as well as by applying pressure<sup>4</sup>. The underdoped compounds show a tetragonal to orthorhombic transition upon cooling followed by an anti-ferromagnetic ordering.

The impact of the rare-earth metal atom substitution on the maximal transition temperature ( $T_{c,max}$ ) achievable by doping is shown in Fig. 2. The optimal starting point for electron doping thus seems to be  $SmFeAsO$  with the highest achievable  $T_c$  for  $REFeAsO_{1-\delta}$ . The influence of the size of the rare-earth metal atom on the structure of  $REFeAsO$  and thereby on superconductivity is essential for the understanding of the mechanism of superconductivity as shown by Kuroki *et al.*<sup>8</sup>, who discussed the height of the arsenic atom above the iron atom layer ( $h_{As}$ ) as a main influence parameter on superconductivity in  $REFeAsO$ .

Precise information on the evolution of the structures with respect to rare-earth metal substitution and oxygen deficiency concentration is therefore important. Structural information is often obtained by Rietveld refinement of powder X-ray diffraction data. While this method yields high quality cell parameters, structural refinement of single-crystal X-ray diffraction data offers a more accurate determination of the structural parameters including displacement parameters.

Single-crystals of  $PrFeAsO$  and  $NdFeAsO$  of  $70\text{--}100\mu m$  have been grown from alkali metal chloride flux<sup>9,10</sup>. By applying pressure also  $SmFeAsO$  single-crystals of up to  $150\mu m$  have been obtained<sup>11,12</sup>. Using high pressure and arsenic as flux Ishikado *et al.* obtained large single-crystals of  $PrFeAsO$ <sup>13</sup>. From pellets of  $NdFeAsO$  and  $LaFeAsO$  synthesized at high pressure Martin *et al.* have been able to isolate crystals with a size up to half a millimeter<sup>14</sup>. Ambient pressure crystal-growth yielding large single-crystals were done by Yan *et al.*<sup>15</sup> for  $LaFeAsO$  using  $NaAs$  and by Jesche *et al.*<sup>16</sup> for  $CeFeAsO$  using  $Sn$  as flux. However, no structural investigation has been conducted on a series of  $RE$ -1111 obtained by the same single-crystal growth technique.

Here we present a new ambient pressure method of single-crystal growth from flux for  $REFeAsO$  ( $RE = La, Ce, Pr, Nd, Sm, Gd, \text{ and } Tb$ ). Atomic parameters were obtained by single-crystal X-ray diffraction and cell parameters were determined by LeBail fits of powder X-ray diffraction data against  $LaB_6$  standard, yielding a consistent set of structural data. Moreover, for the first time anisotropic displacement parameters for the entire series of  $RE$ -1111 are presented. In the light of these data, the influence of the rare-earth metal atom substitution and electron doping on the structural parameters is discussed.

## II. EXPERIMENTAL

The starting materials were handled in an argon-filled glove box (M. Braun,  $p(O_2) \leq 1\text{ ppm}$ ,  $p(H_2O) \leq 1\text{ ppm}$ , argon purification with molecular sieve and copper catalyst). Iron(II)-oxide powder (99.9%, Sigma-Aldrich Chemie GmbH, iron content checked by titration), arsenic (99.999% Alfa Aesar GmbH & Co. KG) and the corresponding, freshly filed rare-earth metal (lanthanum, cerium, praseodymium, neodymium: 99.9%, Treibacher Industrie AG; samarium: 99.9%, Chempur GmbH; gadolinium: 99.9%, ABCR GmbH & Co. KG;

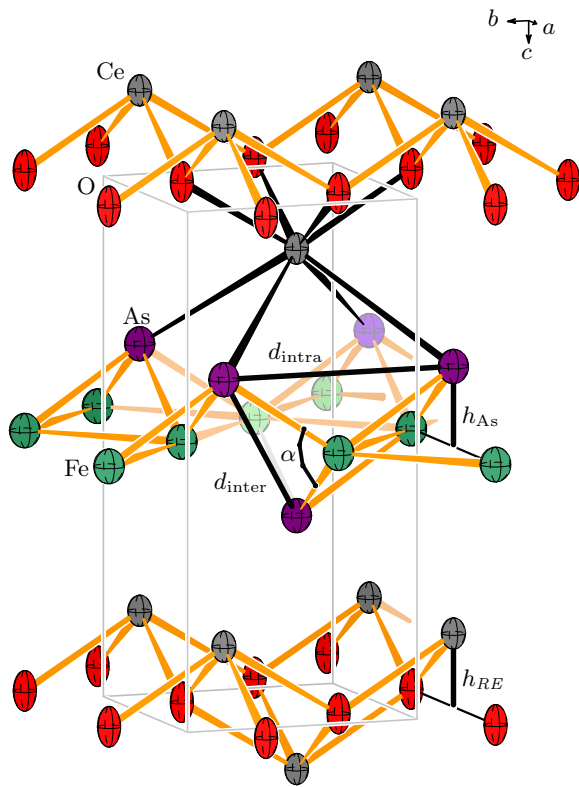


FIG. 1. (color online) Crystal structure of  $\text{CeFeAsO}$  (space group  $P4/nmm$ , no. 129). The displacement ellipsoids represent 95% localization probability. The black bonds emphasize the square anti-prismatic coordination of the rare-earth metal atom by four oxygen atoms and four arsenic atoms.  $h_{\text{As}}$  is the height of the arsenic atoms above the plane of iron atoms.  $h_{\text{RE}}$  is the height of the rare-earth metal atom above the plane of oxygen atoms.  $d_{\text{intra}}$  is the shortest intra-plane distance between two arsenic atoms and equals the lattice parameter  $a$ .  $d_{\text{inter}}$  is the inter-plane distance between two arsenic atoms above and below the iron atom net. The angle  $\alpha$  is often referred to as the tetrahedral angle and indicates the deviation from a tetrahedral coordination of the iron atom.

terbium: 99.9%, Acros Organics BVBA) were mixed and transferred into glassy carbon crucibles. 300–500 wt.-% of the eutectic mixture of NaI/KI (both 99.5%, Grüssing GmbH Analytika, dried at 650 K in dynamic vacuum) was stacked on top of the reactants as flux. Subsequently, the filled crucibles were sealed into silica ampoules under dynamic vacuum. To prevent high arsenic vapor pressures, the ampoules were slowly heated to 1320 K within 24 h. An annealing period of three to six days was applied, followed by slow cooling to 870 K with 1 K/h. After quenching the ampoules in air and removing the flux with deionized water, plate-shaped single-crystals of the  $\text{REFeAsO}$  compounds suitable for structure and transport investigations were obtained.

First attempts to grow single-crystals in accordance with previous studies on  $\text{RETM}_x\text{As}_2$  ( $\text{TM}$  = transition metal)<sup>17</sup> were conducted with rare-earth metal oxide ( $\text{RE}_2\text{O}_3$ ), arsenic, and iron as starting materials and

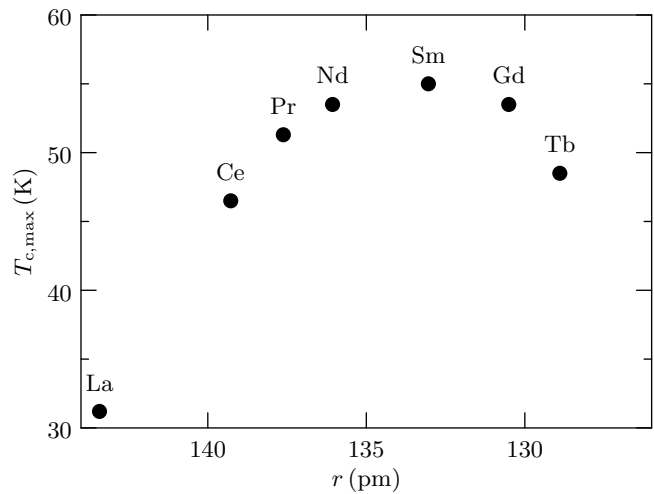


FIG. 2. Evolution of the maximum  $T_c$  for  $\text{REFeAsO}_{1-\delta}$ <sup>5–7</sup> over the effective rare-earth metal atom radii of  $\text{REFeAsO}$ .

alkali metal chlorides as flux. As observed before<sup>12</sup>,  $\text{REOCl}$  hindered the formation of phase-pure samples and single-crystals of the target compounds. The less stable oxide iodides ( $\text{REOI}$ ) are not formed when using sodium or potassium iodide. The exchange of rare-earth metal oxide by iron(III)-oxide or better by iron(II)-oxide as oxygen source, improved single-crystal growth. However, the synthesis of  $\text{REFeAsO}$  with rare-earth metals heavier than terbium failed applying the NaI/KI flux method.

For single-crystal X-ray diffraction smaller crystals were chosen, since larger crystals often showed broad reflection profiles due to stacking faults or mechanical stress as will be discussed later. The single-crystals were isolated and cleaned in inert oil to keep the mechanical stress to a minimum. Subsequently, the crystals were sealed into glass capillaries only immobilized by adhesion to the glass wall by residual oil.

Single-crystal X-ray diffraction data was collected at 293(1) K on a Bruker SMART diffractometer using a molybdenum X-ray source and graphite monochromator ( $\text{Mo K}\alpha$ ). Numerical absorption correction was applied using SADABS<sup>18</sup>. Structure solution and refinement was done with SHELXS and SHELXL<sup>19</sup>, respectively. Further details of the crystal structure investigations may be obtained from Fachinformationszentrum Karlsruhe, 76344 Eggenstein-Leopoldshafen, Germany (fax: (+49)7247-808-666; e-mail: [crysdata@fiz-karlsruhe.de](mailto:crysdata@fiz-karlsruhe.de), <http://www.fiz-karlsruhe.de/>) on quoting the CSD numbers 421998 ( $\text{RE} = \text{La}$ ), 421999 (Ce), 422000 (Pr), 422001 (Nd), 422002 (Sm), 422003 (Gd), and 422004 (Tb).

$\omega$ -scans of single reflections were done with APEX2<sup>20</sup> by rotating  $1^\circ$ . The crystals were cooled with a nitrogen gas stream using a Cryostream Controller 700 by Oxford Cryosystems for low temperature  $\omega$ -scans.

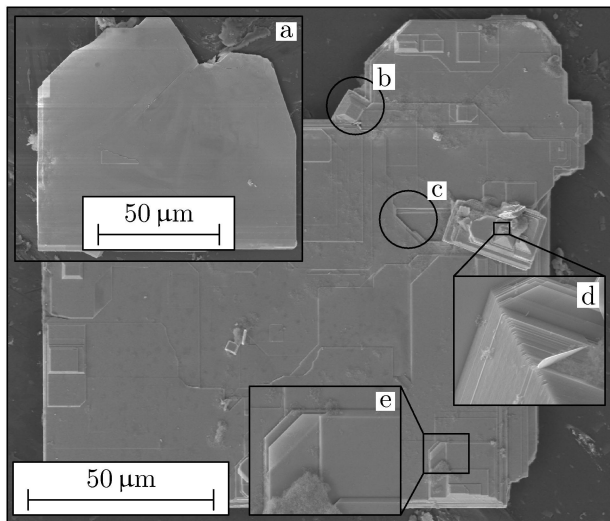


FIG. 3. (a) Scanning electron microscope (SEM) image of a NdFeAsO crystal used for single-crystal X-ray diffraction studies. (b-e) SEM image of a GdFeAsO crystal showing common growth instabilities of larger crystals: (b) additional crystal intergrown in random orientation, (c-e) free grown planes.

Powder X-ray diffraction patterns were measured at 293(1) K on a Stadi P diffractometer (Stoe & Cie., Darmstadt, Cu  $K\alpha_1$ , Ge monochromator). Lattice constants were refined by a LeBail pattern decomposition against an internal LaB<sub>6</sub>-standard using GSAS<sup>21</sup> and EXPGUI<sup>22</sup>. Pseudo-Voigt profile functions with a model for axial divergence were applied to fit the measured data.

Growth features, crystal composition, and flux incorporation were checked by scanning electron microscopy and energy dispersive X-ray spectroscopy (EDX) at an Ultra55 FEG-microscope (Carl Zeiss NTS GmbH) with a XFlash EDX-detector 4010 (SDD) assembling a Quantax 400 (Bruker AXS Microanalysis GmbH). The EDX-detector was calibrated with germanium standard.

Electrical resistivity measurements were carried out in a standard four probe geometry in the temperature range of 1.8–300 K by using a commercial physical property measurement system (PPMS, Quantum Design).

### III. RESULTS

Single-crystals suitable for X-ray diffraction measurements were obtained for all  $REFeAsO$  ( $RE = \text{La, Ce, Pr, Nd, Sm, Gd, and Tb}$ ). Larger crystals were observed especially for the heavier rare-earth metals Gd and Tb. Whereas the size generally ranged from 30 to 300  $\mu\text{m}$  for all  $RE$ -1111, a crystal of half a millimeter size was obtained for TbFeAsO.

Fig. 3 depicts the usual growth features of the single-crystals. The crystal growth for  $REFeAsO$  is generally much faster in the  $ab$ -plane than along the  $c$ -axis. Ac-

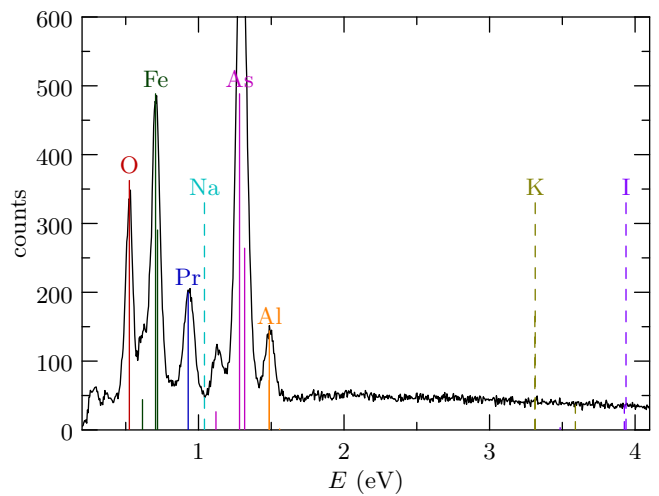


FIG. 4. (color online) EDX spectrum of PrFeAsO. Characteristic lines of the elements of the flux (positions marked by dashed lines) are not observed. The aluminum signal originates from the specimen holder.

cordingly, the platelets with a length of up to 300  $\mu\text{m}$  are only few microns thick rendering the crystals very fragile. Mechanical stresses can easily lead to bending, splitting, or fracture of the crystal, which causes broad reflection profiles in single-crystal X-ray diffraction. Additionally, the larger crystals often show free growing planes (Fig. 3 c-e), which can cause flux incorporation. Furthermore, intergrowth of crystals in random orientation to the main crystal (Fig. 3 b) was observed for larger crystals, hampering single-crystal X-ray diffraction investigations. Smaller single-crystals (Fig. 3 a) are of better quality, resulting in acceptable full width at half-maximum of the Bragg reflections.

Within the accuracy of the EDX measurement the composition of the crystals was proved to be 1:1:1:1. Characteristic emission lines of neither potassium nor iodine were observed, thus substantial inclusion or incorporation of the flux material can be excluded. Yet the case of sodium is more complex, since the emission lines are often covered by the signal of the rare-earth metals. However, in the case of PrFeAsO also sodium could definitively be excluded, as can be seen in Fig. 4.

The parameters of single-crystal X-ray diffraction data collections and the results of the crystal structure refinements of the quaternary iron pnictides are presented in Tab. I. The lattice parameters from powder diffraction and atomic data from single-crystal diffraction are compiled in Tab. II.

Using NaI/KI-flux we obtained single-crystals, which are not only sufficient for crystallographic investigations but also large enough to measure the electrical resistivity along the basal plane with a standard four-probe geometry (Fig. 5, inset). Over the entire temperature range the resistivity of TbFeAsO varies only between 0.85 and 1.05 m $\Omega\text{cm}$ . The room-temperature resistiv-

TABLE I. Parameters of single-crystal X-ray diffraction data collection at 293(1) K and results of the structural refinement of  $REFeAsO$ .

$RE$	$\theta_{\max}$ (°)	$R_{\text{int}}$	$R_{\sigma}$	$R_1$	$wR_2$	$S$	$\Delta\rho_{\max, \min}$ ( $e^- \text{ \AA}^{-3}$ )
La	37.52	0.037	0.016	0.027	0.023	2.22	1.69, -1.59
Ce	37.57	0.034	0.016	0.024	0.025	2.28	1.52, -1.87
Pr	37.65	0.039	0.017	0.025	0.018	1.66	2.01, -2.70
Nd	39.78	0.017	0.009	0.018	0.018	3.11	1.74, -1.15
Sm	37.57	0.024	0.010	0.011	0.013	1.92	0.89, -1.41
Gd	37.66	0.025	0.016	0.024	0.025	2.58	2.23, -2.25
Tb	37.52	0.018	0.009	0.012	0.016	2.51	1.20, -1.04

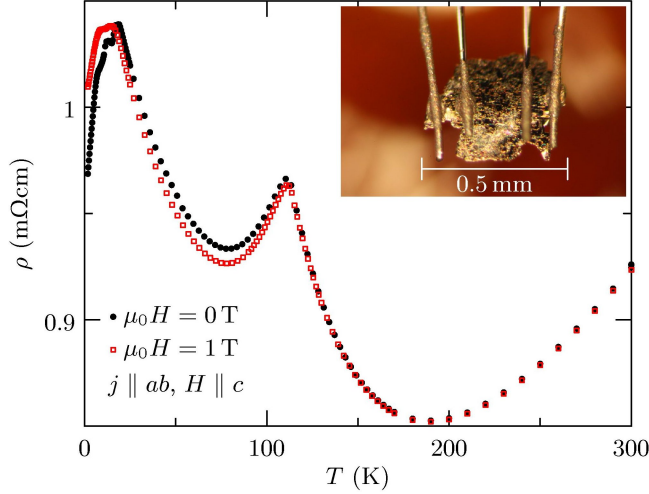


FIG. 5. (color online) Temperature dependence of the electrical resistivity of a  $TbFeAsO$  single-crystal (shown in the inset) in the  $ab$ -plane. The local maximum at  $T_S = 112$  K results from a structural transition.

ity,  $\rho_{300\text{ K}} \approx 1 \text{ m}\Omega\text{cm}$ , indicates poor metallicity. Upon cooling the resistivity of  $TbFeAsO$  passes a minimum at about 180 K towards a local maximum centered at  $T_S = 112$  K, marking the structural transition and the magnetic ordering of iron, which occurs at a slightly lower temperature than reported for polycrystalline material ( $T = 122 \text{ K}^{24}$ ). Below  $T = 75$  K,  $\rho(T)$  increases again, showing similarities to  $LaFeAsO^2$ , followed by a decrease at  $T < 18$  K. The decrease of  $\rho(T)$  changes slope towards lower temperature with a linear temperature dependence at  $T < 6$  K. The onset of the anomaly at  $T \approx 20$  K is also observable in polycrystalline material where no data is reported for  $T \leq 19 \text{ K}^{24}$ . A similar behavior was published for  $NdFeAsO$ , where the change of the magnetic structure of Fe at  $T = 15$  K results in a significant decrease in the electrical resistivity of single-crystalline material with the current in the  $ab$ -plane<sup>25</sup>. The  $TbFeAsO$  single-crystal measured (Fig. 5) has a thickness of only 10  $\mu\text{m}$  and is accordingly sensitive to strain caused by the wires and silver-paint contacts. Small deformation can result in cracks along the sample, which might be responsible for the observed differences

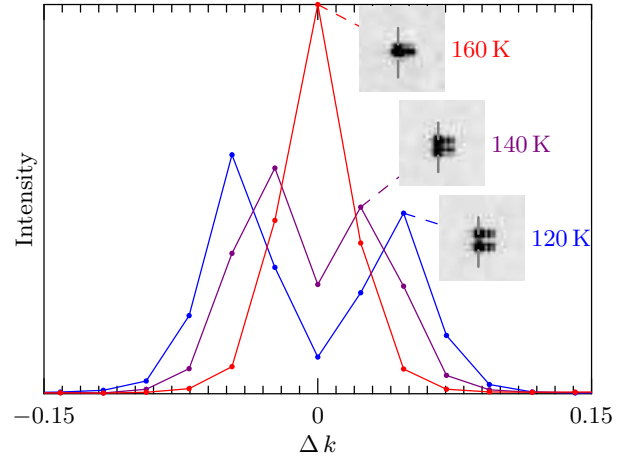


FIG. 6. (color online)  $\omega$ -scan of the  $Mo K\alpha_1$  and  $K\alpha_2$  Bragg reflections 800 of  $LaFeAsO$  showing a splitting on cooling below the tetragonal to orthorhombic transition. Lines are guides for the eye. The data points correspond to the resolution of the area detector.

to polycrystalline material. Applying a magnetic field of  $\mu_0 H = 1$  T has no significant influence on the structural transition at  $T_S$  and leads to a small negative magnetoresistance at lower temperatures. The decrease in the electrical resistivity occurring at  $T = 18$  K in zero field is shifted to  $T = 14$  K.

Splitting of the tetragonal Bragg reflection 800 occurring below 160 K is demonstrated exemplarily for  $LaFeAsO$  (Fig. 6), indicating the structural transition from space group  $P4/nmm$  to  $Cmme$  as expected for undoped  $LaFeAsO$ .<sup>26</sup>

#### IV. DISCUSSION

To assess the influence of the rare-earth metal substitution on the structure of  $RE$ -1111 and thereby on superconductivity, a suitable scale has to be defined. Often, the radii of the substituted atoms are used since a linear correlation to the volume of the structure is expected in analogy to Vegard's law.

As depicted in Fig. 1, the rare-earth metal atom is coordinated by four oxygen atoms and four arsenic atoms. This suggests the use of the radii for eight-fold coordinated  $RE^{3+}$  ions as revised by Shannon<sup>23</sup> and originally deduced by Greis and Petzel<sup>27</sup> from the nine-fold coordination in  $REF_3$  where the coordination polyhedron is assembled by equal anions at almost equal distances.

However, in  $REFeAsO$  the square spanned by the four arsenic atoms is twice as large as the square spanned by the oxygen atoms, leading to a strong distortion of the square anti-prism with a large difference in cation-anion distances ( $\bar{d}_{RE-O} \approx 230 \text{ pm}$ ,  $\bar{d}_{RE-As} \approx 330 \text{ pm}$ ). The more inhomogeneous coordination in  $REFeAsO$  compared to the coordination in  $REF_3$  creates a deviation from linearity of the volume evolution over the chosen rare-earth

TABLE II. Structural parameters of  $REFeAsO$  in space group  $P4/nmm$  (No. 129) and  $Z = 2$  measured at 293(1) K. Cell parameters were determined by LeBail fits of powder X-ray diffraction patterns. Atomic positions and anisotropic displacement parameters were refined from single-crystal X-ray diffraction data.

$RE$	$r$ (pm) <sup>b</sup>	$a$ (pm)	$c$ (pm)	$RE^a$		As		Fe		O	
				$z$	$U_{11}^c$	$U_{33}$	$z$	$U_{11}$	$U_{33}$	$U_{11}$	$U_{33}$
La	130	403.67(1)	872.18(4)	0.14141(5)	57(1)	85(2)	0.65138(9)	85(2)	107(4)	88(3)	106(5)
Ce	128.3	400.58(1)	862.89(6)	0.14106(4)	50(1)	85(2)	0.65442(8)	79(2)	102(3)	81(3)	105(5)
Pr	126.6	398.89(1)	859.66(8)	0.13960(4)	62(1)	96(2)	0.65608(7)	86(2)	107(3)	87(2)	121(4)
Nd	124.9	397.13(1)	856.55(5)	0.13899(3)	61(1)	93(1)	0.65725(6)	85(2)	107(3)	84(2)	109(4)
Sm	121.9	394.69(2)	849.65(6)	0.13705(2)	56(1)	88(1)	0.66007(4)	80(1)	96(2)	78(2)	108(3)
Gd	119.3	391.99(3)	844.51(8)	0.13570(5)	69(1)	98(2)	0.6623(1)	92(2)	109(5)	93(4)	112(7)
Tb	118	390.43(3)	840.8(1)	0.13455(3)	57(1)	69(1)	0.66389(6)	80(1)	76(3)	76(2)	100(4)

<sup>a</sup>  $RE$ , As:  $2c$ ,  $x = 1/4$ ,  $y = 1/4$ ,  $z$ ; Fe:  $2b$ ,  $x = 3/4$ ,  $y = 1/4$ ,  $z = 1/2$ ; O:  $2a$ ,  $x = 3/4$ ,  $y = 1/4$ ,  $z = 0$

<sup>b</sup> Radii of the corresponding trivalent rare-earth metal in octahedral coordination from Ref. 23

<sup>c</sup> All  $U_{ij}$  in  $\text{pm}^2$ ,  $U_{11} = U_{22}$ ,  $U_{12} = U_{23} = U_{13} = 0$

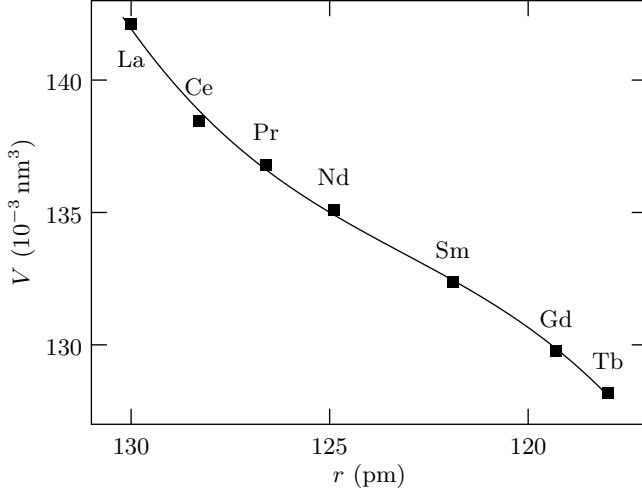


FIG. 7. Unit cell volume of  $REFeAsO$  over the rare-earth metal radii as compiled by Shannon<sup>23</sup> for eight-fold coordinated trivalent ions. The errorbars are within the size of the symbols.

metal radii in eight-fold coordination as shown in Fig. 7.

Thorough investigation of the crystal structures of  $RE$ -1111 reveals, that the inter-plane distance of the arsenic atoms (Fig. 1) is constant(!),  $d_{\text{inter}} = 389.4(4)$  pm. It appears to be the minimum distance arsenic atoms can attain in undoped  $REFeAsO$  ( $RE = \text{La, Ce, Pr, Nd, Sm, Gd, and Tb}$ ). The intra-plane distance of the arsenic atoms,  $d_{\text{intra}}$  (Fig. 1), is equal to the  $a$ -axis, and longer than  $d_{\text{inter}}$ . Going from lanthanum to terbium as depicted in Fig. 8, the intra-plane distance approaches the inter-plane distance of the arsenic atoms preventing a further shrinkage of the structure. Consequently, all  $REFeAsO$  compounds with smaller rare-earth metal atoms ( $RE = \text{Dy, Ho, ...}$ ) have to be synthesized under external pressure as described in literature<sup>9,28,29</sup>.

The iron-arsenic layer in  $TbFeAsO$  can thus be considered as a section of a body centered cubic packing of

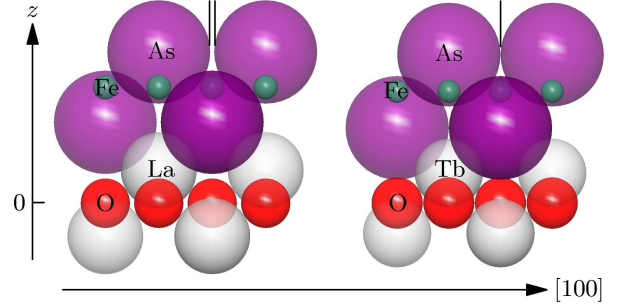


FIG. 8. (color online) Hard-sphere model representation of  $LaFeAsO$  (left) and  $TbFeAsO$  (right). The intra-plane distance (see Fig. 1) of the arsenic atoms approaches the inter-plane distance going from lanthanum to terbium.

arsenic atoms with iron atoms situated in the tetrahedral voids.

With  $d_{\text{inter}}$  being constant over the rare-earth substitution and the interaction between  $RE$ , As and O being predominantly ionic, as argued by Blanchard *et al.*<sup>30</sup>, the structure of  $REFeAsO$  can be analyzed in a hard-sphere model (Fig. 8). The radius of the arsenic sphere is  $r_{\text{As}} = \frac{1}{2} d_{\text{inter}}$ . The radius of the iron sphere is deduced from the shortest inter-atomic distance of iron and arsenic atoms  $r_{\text{Fe}} = d_{\text{As-Fe}} - r_{\text{As}}$ . The same can be done for the radius of the rare-earth metal sphere ( $r_{\text{RE}} = d_{\text{As-RE}} - r_{\text{As}}$ ). The radius of the oxygen sphere cannot be determined directly from  $d_{\text{inter}}$  and has to be calculated from the radius of the rare-earth metal sphere and the shortest inter-atomic distance of oxygen and rare-earth metal atom ( $r_{\text{O}} = d_{\text{RE-O}} - r_{\text{RE}}$ ).

The resulting effective radii are listed in Tab. III. According to the hard-sphere model, all radii except those of the rare-earth metal atoms should be almost constant. Indeed, the deviations in the calculated values are small, yet exhibit the limits of the model, which does not account for polarization effects or covalent bonding. Nevertheless, the changes of the rare-earth metal atom radii ( $r_{\text{RE}}$ ) are an order of magnitude larger than those of



TABLE III. Calculated effective radii of the atoms in  $REFeAsO$  as deduced from the hard-sphere model. The errors are estimated by combined variances.

$RE$	$r_{RE}$ (pm)	$r_{Fe}$ (pm)	$r_{As}^a$ (pm)	$\frac{1}{2}a^b$ (pm)	$r_O$ (pm)
La	143.42(9)	46.76(7)	194.42(6)	201.84(1)	93.12(9)
Ce	139.28(8)	46.11(7)	194.46(5)	200.29(1)	95.10(8)
Pr	137.62(8)	45.72(6)	194.66(5)	199.45(1)	95.15(8)
Nd	136.06(6)	45.37(5)	194.57(4)	198.57(1)	95.45(6)
Sm	133.17(5)	44.81(4)	194.86(3)	197.35(1)	95.97(5)
Gd	130.5(1)	44.2(1)	194.94(7)	196.00(2)	96.5(1)
Tb	128.90(7)	43.90(6)	195.05(5)	195.22(2)	96.73(8)

<sup>a</sup>  $r_{As} = \frac{1}{2} d_{inter}$   
<sup>b</sup>  $\frac{1}{2} a = \frac{1}{2} d_{intra}$

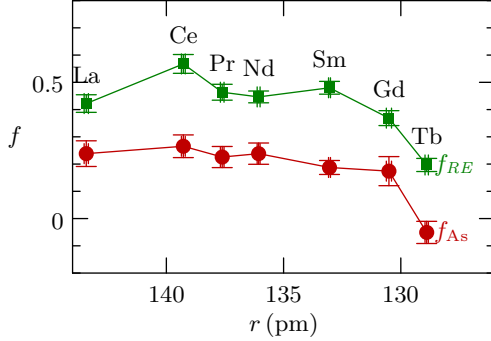


FIG. 9. (color online) Anisotropy of vibration  $f$  of the arsenic and rare-earth atoms in  $REFeAsO$  with  $f = 0$  indicating an isotropic vibraional behavior. Connecting lines are guides for the eye. Errorbars by combined variances.

the other atoms. The above mentioned geometrical limit of the  $REFeAsO$  series with  $RE = Tb$  can clearly be seen by the equalization of  $d_{intra} \equiv a$  and  $d_{inter} \equiv 2r_{As}$

Additionally, the sphere packing can be checked by the anisotropy of vibration

$$f = \frac{U_{33} - U_{11}}{(2U_{11} + U_{33})/3},$$

which indicates the elongation of the displacement ellipsoid along the  $c$ -axis, with  $f = 0$  referring to an isotropic vibration. For all  $RE$  the arsenic atom shows almost the same anisotropy of vibration (Fig. 9). Only for the densely packed situation of  $TbFeAsO$  isotropic displacement is observed. For the vibration of the heavier rare-earth atoms the trend towards diminished anisotropy is observed, too.

Using the effective radii of  $RE$  as a scale to compare the influence of the rare-earth metal substitution on the structure of  $RE$ -1111 leads to a linear evolution of structural features such as the volume or the height of the arsenic atom over the square iron-net (Fig. 10). Although  $LaFeAsO$  fits the linear evolution of the volume of  $REFeAsO$ , it deviates slightly from the linear trends in the height of the arsenic atom over the square iron-net ( $h_{As} = [z_{As} - 0.5] c$ ) and in the height of the rare-

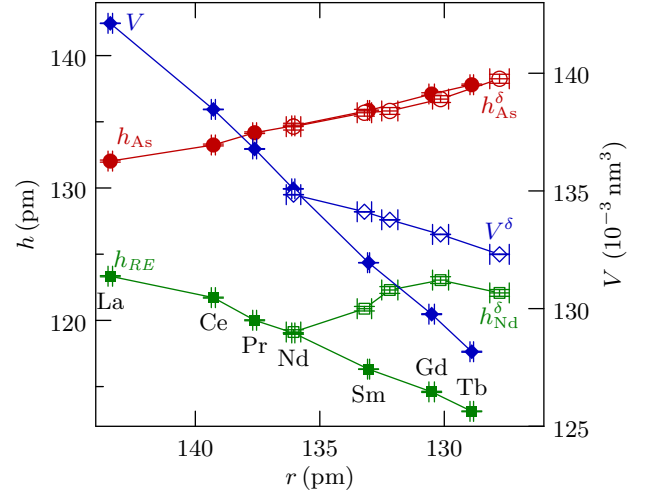


FIG. 10. (color online) The height of the arsenic atom ( $h_{As}$  see Fig. 1) over the iron plane, the height of the rare-earth metal atom ( $h_{RE}$  see Fig. 1) over the oxygen layer and the volume  $V$  over the effective radii of the trivalent rare-earth metal deduced from the hard-sphere model. The open symbols represent data for  $NdFeAsO_{1-\delta}$ <sup>31</sup>. From left to right:  $\delta = 0.05(1)$ , RT, non-superconducting;  $\delta = 0.080(9)$ , RT,  $T_c = 35$  K;  $\delta = 0.14(1)$ , RT,  $T_c = 44$  K;  $\delta = 0.17(1)$ , RT,  $T_c = 51$  K;  $\delta = 0.17(1)$ , 10 K,  $T_c = 51$  K. Connecting lines are guides for the eye. Errorbars by combined variances.

earth metal atom over the oxygen layer ( $h_{RE} = z_{RE} c$ ). Since the radius for the rare-earth metal atom is deduced from the inter-atomic distance of arsenic and the rare-earth metal, closer coordination towards oxygen than expected from linear extrapolation results in a comparatively large effective radius for the  $f^0$ -cation  $La^{3+}$  (Tab. III). This is consistent with the larger decrease of  $T_{c,max}$  from  $CeFeAsO_{1-\delta}$  (46.5 K) to  $LaFeAsO_{1-\delta}$  (31.2 K) compared to the decrease from  $PrFeAsO_{1-\delta}$  (51.3 K)<sup>5</sup> to  $CeFeAsO_{1-\delta}$  as can be seen in Fig. 2.

The exceptional position of  $LaFeAsO$  can also be observed in the normalized inter-atomic distances  $D$  as depicted in Fig. 11. The largest changes in inter-atomic distances are observed for the interactions directly influenced by the rare-earth metal substitution:  $d_{RE-As}$ ,  $d_{RE-O}$  and  $d_{intra}$  decrease monotonically, with the latter corresponding to the  $a$ -parameter. The inter-atomic distances between iron and arsenic (not shown in the Figure) and the inter-plane distance of the arsenic atoms are almost invariant to rare-earth metal substitution.

To assess the influence of oxygen vacancy concentration on the structure of  $REFeAsO$ , literature data for  $NdFeAsO_{1-\delta}$  from Lee *et al.*<sup>31</sup> were also evaluated with the hard-sphere model (open symbols in Fig. 10 and Fig. 11). Oxygen deficiency weakens the bonding in the NdO layer. The distance between oxygen and neodymium atoms as well as  $h_{Nd}^{\delta}$  increases slightly. The weaker Nd-O bonding, respectively the higher charge of the  $(NdO_{1-\delta})^{(1+2\delta)+}$  and  $(FeAs)^{(1+2\delta)-}$  layers is compensated by stronger Nd-As bonding. The shorter  $d_{Nd-As}^{\delta}$

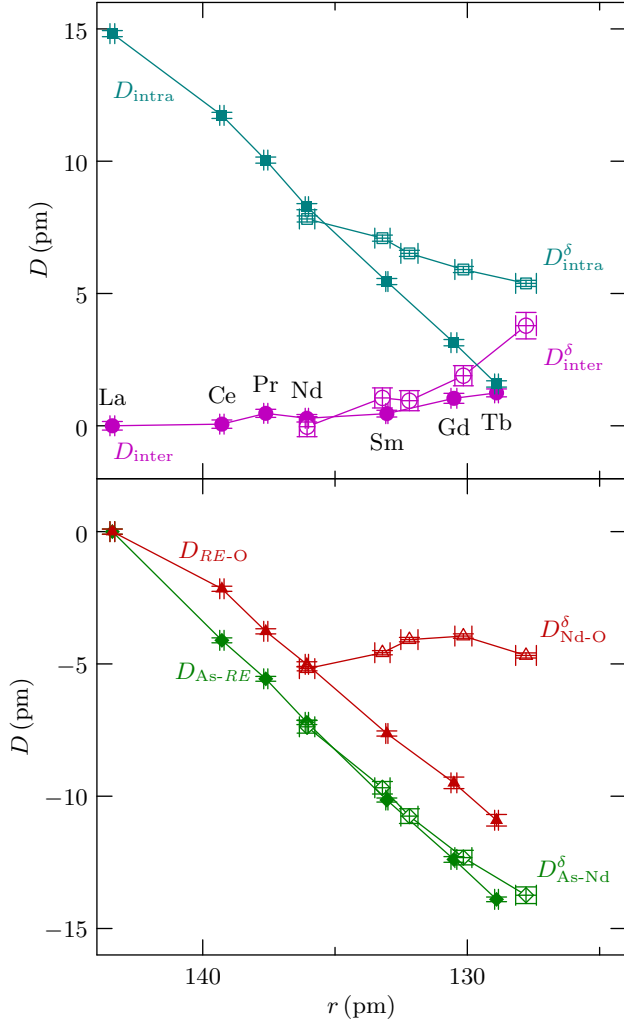


FIG. 11. (color online) Plot of the normalized inter-atomic distances  $D_{\text{A-B}} = d_{\text{A-B}}^{\text{REFeAsO}} - d_{\text{A-B}}^{\text{LaFeAsO}}$  with respect to LaFeAsO over the calculated effective rare-earth atom radii deduced from the hard-sphere model. For better comparison of the normalized intra- and inter-plane distance of the arsenic atoms,  $D_{\text{intra}}$  is calculated by  $d_{\text{intra}}^{\text{REFeAsO}} - d_{\text{inter}}^{\text{LaFeAsO}}$ . The open symbols represent data for NdFeAsO $_{1-\delta}$ <sup>31</sup>. From left to right:  $\delta = 0.05(1)$ , RT, non-superconducting;  $\delta = 0.080(9)$ , RT,  $T_c = 35$  K;  $\delta = 0.14(1)$ , RT,  $T_c = 44$  K;  $\delta = 0.17(1)$ , RT,  $T_c = 51$  K;  $\delta = 0.17(1)$ , 10 K,  $T_c = 51$  K. Connecting lines are guides to the eye. Errorbars by combined variances.

results in smaller  $r_{\text{Nd}}$ . Concurrently, the distance of arsenic atoms to the iron layer  $h_{\text{As}}^\delta$  is enlarged. As the inter-plane As-As distance increases, the geometrical limit of the structure type is changed. Further contraction (here due to cooling from RT to 10 K) leads again to the equalization of  $d_{\text{inter}}$  and  $d_{\text{intra}}$ , however at a value that is about 4 pm larger.

As depicted by Lee *et al.*<sup>31</sup>, the angle  $\alpha$  of the doped REFeAsO compounds at low temperatures is a reasonable indicator for  $T_{c,\text{max}}$ , which is highest for the tetrahedral angle of  $109.5^\circ$ . However, the structural argu-

ments do not suffice. Taking LaFeAsO $_{1-x}\text{F}_x$  as an example, doping triggers superconductivity at  $x \approx 0.05$ , with  $T_{c,\text{max}} \approx 24$  K at  $x \approx 0.1$ , and a subsequent suppression of superconductivity at higher doping levels<sup>32</sup>. Geometrically, the increase in doping should further increase  $\alpha$  towards the ideal tetrahedral coordination for the iron atoms, with a further increase in  $T_c$ . It can thus be argued that high- $T_c$  values originate from a coincidence of electronic and structural optima.

Comparing the influence of rare-earth substitution exemplarily with the data of oxygen deficiency doping data of Lee *et al.* shows the high impact of electronic doping on the structure. Kuroki *et al.*<sup>8</sup> indicated the strong influence of  $h_{\text{As}}$  on the electronic structure of RE-1111. It was predicted that the combination of large cell volume  $V$  and increased height of the arsenic atom  $h_{\text{As}}$  results in high  $T_c$ . As can be deduced from the diametric trends in Fig. 10, a medium sized rare-earth metal atom in combination with a large oxygen deficiency should be used. In accordance with experimental data, NdFeAsO $_{1-\delta}$  seems to be close to the optimum.

## V. CONCLUSIONS

Using alkali metal iodides as flux facilitated the free growth of REFeAsO ( $\text{RE} = \text{La}, \text{Ce}, \text{Pr}, \text{Nd}, \text{Sm}, \text{Gd}$ , and  $\text{Tb}$ ) single-crystals suitable for resistivity measurements and single-crystal X-ray diffraction studies. The elaborated consistent set of structural data for the RE-1111 compounds and the comparison with structural data of NdFeAsO $_{1-\delta}$  from literature allowed a thorough investigation of the influence of the rare-earth metal substitution and doping on the structural features of RE-1111.

A hard-sphere model proved to be suitable for the interpretation of structural trends. The thereby revealed geometrical limit for the structure type rationalizes the failure of ambient pressure synthesis of heavier RE-1111 then TbFeAsO.

Additionally, an interplay of electronic and structural optima for high- $T_c$  values is proposed.

The structural data also provide a reliable basis for theoretical investigations of the electronic structure of the undoped compounds and their relation to their superconducting congeners.

Further single-crystal studies of doped REFeAsO compounds and the evolution over the temperature will help to complete the geometrical model of the iron-based superconductors.

## VI. ACKNOWLEDGMENT

The authors like to thank Jutta Krug, Alexander Gerisch, and Tilmann Meusel for their help with sample preparation and measurements.

- <sup>1</sup> Y. Kamihara, H. Hiramatsu, M. Hirano, R. Kawamura, H. Yanagi, T. Kamiya, and H. Hosono, *J. Am. Chem. Soc.*, **128**, 10012 (2006).
- <sup>2</sup> Y. Kamihara, T. Watanabe, M. Hirano, and H. Hosono, *J. Am. Chem. Soc.*, **130**, 3296 (2008).
- <sup>3</sup> H.-H. Wen, G. Mu, L. Fang, H. Yang, and X. Zhu, *Europhys. Lett.*, **82**, 17009 (2008).
- <sup>4</sup> H. Takahashi, H. Okada, K. Igawa, Y. Kamihara, M. Hirano, and H. Hosono, *Physica C*, **469**, 413 (2009).
- <sup>5</sup> Z.-A. Ren, G.-C. Che, X.-L. Dong, J. Yang, W. Lu, W. Yi, X.-L. Shen, Z.-C. Li, L.-L. Sun, F. Zhou, and Z.-X. Zhao, *Europhys. Lett.*, **83**, 17002 (2008).
- <sup>6</sup> J. Yang, Z.-C. Li, W. Lu, W. Yi, X.-L. Shen, Z.-A. Ren, G.-C. Che, X.-L. Dong, L.-L. Sun, F. Zhou, and Z.-X. Zhao, *Supercond. Sci. Tech.*, **21**, 082001 (2008).
- <sup>7</sup> J. Yang, X.-L. Shen, W. Lu, W. Yi, Z. C. Li, Z.-A. Ren, G.-C. Che, X.-L. Dong, L.-L. Sun, F. Zhou, and Z.-X. Zhao, *New J. Phys.*, **11**, 025005 (2009).
- <sup>8</sup> K. Kuroki, H. Usui, S. Onari, R. Arita, and H. Aoki, *Phys. Rev. B*, **79**, 224511 (2009).
- <sup>9</sup> P. Quebe, L. J. Terbuchte, and W. Jeitschko, *J. Alloy. Compd.*, **302**, 70 (2000).
- <sup>10</sup> L. Fang, P. Cheng, Y. Jia, X. Zhu, H. Luo, G. Mu, C. Gu, and H.-H. Wen, *J. Cryst. Growth*, **311**, 358 (2009).
- <sup>11</sup> N. D. Zhigadlo, S. Katrych, Z. Bukowski, S. Weyeneth, R. Puzniak, and J. Karpinski, *J. of Phys.-Condens. Mat.*, **20**, 342202 (2008).
- <sup>12</sup> J. Karpinski, N. D. Zhigadlo, S. Katrych, Z. Bukowski, P. Moll, S. Weyeneth, H. Keller, R. Puzniak, M. Tortello, D. Daghero, R. Gonnelli, I. Maggio-Aprile, Y. Fasano, O. Fischer, K. Rogacki, and B. Batlogg, *Physica C*, **469**, 370 (2009).
- <sup>13</sup> M. Ishikado, S. Shamoto, H. Kito, A. Iyo, H. Eisaki, T. Ito, and Y. Tomioka, *Physica C*, **469**, 901 (2009).
- <sup>14</sup> C. Martin, M. E. Tillman, H. Kim, M. A. Tanatar, S. K. Kim, A. Kreyssig, R. T. Gordon, M. D. Vannette, S. Nandi, V. G. Kogan, S. L. Bud'ko, P. C. Canfield, A. I. Goldman, and R. Prozorov, *Phys. Rev. Lett.*, **102**, 247002 (2009).
- <sup>15</sup> J.-Q. Yan, S. Nandi, J. L. Zarestky, W. Tian, A. Kreyssig, B. Jensen, A. Kracher, K. W. Dennis, R. J. McQueeney, A. I. Goldman, R. W. McCallum, and T. A. Lograsso, *Applied Physics Letters*, **95**, 222504 (2009).
- <sup>16</sup> A. Jesche, C. Krellner, M. de Souza, M. Lang, and C. Geibel, *New J. Phys.*, **11**, 103050 (2009).
- <sup>17</sup> D. Rutzinger, C. Bartsch, M. Doerr, H. Rosner, V. Neu, T. Doert, and M. Ruck, *J. Solid State Chem.*, 527 (2009).
- <sup>18</sup> G. M. Sheldrick, "SADABS (Version 2008/1), Bruker AXS Inc." (2008).
- <sup>19</sup> G. M. Sheldrick, *Acta Crystallogr. A*, **64**, 112 (2007).
- <sup>20</sup> "APEX2 (Version 2009.9), Bruker AXS Inc." (2009).
- <sup>21</sup> A. C. Larson and R. B. V. Dreele, *LAUR*, **86-748** (2000).
- <sup>22</sup> B. H. Toby, *J. Appl. Crystallogr.*, **34**, 210 (2001).
- <sup>23</sup> R. D. Shannon, *Acta Crystallogr. A*, **32**, 751 (1976).
- <sup>24</sup> Y. Luo, Q. Tao, Y. Li, X. Lin, L. Li, G. Cao, Z.-A. Xu, Y. Xue, H. Kaneko, A. V. Savinkov, H. Suzuki, C. Fang, and J. Hu, *Phys. Rev. B*, **80**, 224511 (2009).
- <sup>25</sup> W. Tian, W. Ratcliff II, M. G. Kim, J.-Q. Yan, P. A. Kienle, Q. Huang, B. Jensen, K. W. Dennis, R. W. McCallum, T. A. Lograsso, R. J. McQueeney, A. I. Goldman, J. W. Lynn, and A. Kreyssig, "Interplay between Fe and Nd magnetism in NdFeAsO single crystals," (2010), arXiv:cond-mat/1006.1135.
- <sup>26</sup> C. de la Cruz, Q. Huang, J. W. Lynn, J. Li, W. Ratcliff II, J. L. Zarestky, H. A. Mook, G. F. Chen, J. L. Luo, N. L. Wang, and P. Dai, *Nature*, **453**, 899 (2008).
- <sup>27</sup> O. Greis and T. Petzel, *Z. Anorg. Allg. Chem.*, **403**, 1 (1974).
- <sup>28</sup> J.-W. G. Bos, G. B. S. Penny, J. A. Rodgers, D. A. Sokolov, A. D. Huxley, and J. P. Attfield, *Chemical Communications*, 3634 (2008).
- <sup>29</sup> J. A. Rodgers, G. B. S. Penny, A. Marcinkova, J.-W. G. Bos, D. A. Sokolov, A. Kusmartseva, A. D. Huxley, and J. P. Attfield, *Phys. Rev. B*, **80**, 052508 (2009).
- <sup>30</sup> P. E. R. Blanchard, R. G. Cavell, and A. Mar, *J. Solid State Chem.*, **183**, 1477 (2010).
- <sup>31</sup> C. H. Lee, A. Iyo, H. Eisaki, H. Kito, M. T. Fernandez-Diaz, T. Ito, K. Kihou, H. Matsuhata, M. Braden, and K. Yamada, *J. Phys. Soc. Jpn.*, **77**, 083704 (2008).
- <sup>32</sup> H. Luetkens, H.-H. Klauss, M. Kraken, F. J. Litterst, T. Dellmann, R. Klingeler, C. Hess, R. Khasanov, A. Amato, C. Baines, M. Kosmala, O. J. Schumann, M. Braden, J. Hamann-Borrero, N. Leps, A. Kondrat, G. Behr, J. Werner, and B. Buchner, *Nature Materials*, **8**, 305 (2009).